

Stability of the M2 phase of vanadium dioxide induced by coherent epitaxial strain

N. F. Quackenbush,¹ H. Paik,² M. J. Wahila,¹ S. Sallis,³ M. E. Holtz,^{4,5} X. Huang,⁶ A. Ganose,^{7,8} B. J. Morgan,⁹ D. O. Scanlon,^{7,8} Y. Gu,¹⁰ F. Xue,¹⁰ L.-Q. Chen,¹⁰ G. E. Sterbinsky,^{11,*} C. Schlueter,⁸ T.-L. Lee,⁸ J. C. Woicik,¹² J.-H. Guo,¹³ J. D. Brock,^{6,14} D. A. Muller,^{4,5} D. A. Arena,¹⁵ D. G. Schlom,^{2,5} and L. F. J. Piper^{1,3,†}

¹*Department of Physics, Applied Physics and Astronomy, Binghamton University, Binghamton, New York 13902, USA*

²*Department of Materials Science and Engineering, Cornell University, Ithaca, New York 14853-1501, USA*

³*Materials Science & Engineering, Binghamton University, Binghamton, New York 13902, USA*

⁴*School of Applied and Engineering Physics, Cornell University, Ithaca, New York 14853, USA*

⁵*Kavli Institute at Cornell for Nanoscale Science, Ithaca, New York 14853, USA*

⁶*School of Applied and Engineering Physics, Cornell University, Ithaca, New York 14853-1501, USA*

⁷*University College London, Kathleen Lonsdale Materials Chemistry, Department of Chemistry,*

20 Gordon Street, London WC1H 0AJ, United Kingdom

⁸*Diamond Light Source Ltd., Harwell Science and Innovation Campus, Didcot, Oxfordshire OX11 0DE, United Kingdom*

⁹*Department of Chemistry, University of Bath, Claverton Down, Bath BA2 7AY, United Kingdom*

¹⁰*Department of Materials Science and Engineering, The Pennsylvania State University, University Park, Pennsylvania 16803, USA*

¹¹*National Synchrotron Light Source, Brookhaven National Laboratory, Upton, New York 11973, USA*

¹²*Materials Science and Engineering Laboratory, National Institute of Standards and Technology, Gaithersburg, Maryland 20899, USA*

¹³*Advanced Light Source, Lawrence Berkeley National Laboratory, Berkeley, California, USA*

¹⁴*Cornell High Energy Synchrotron Source, Cornell University, Ithaca, New York 14853-1501, USA*

¹⁵*Department of Physics, University of South Florida, Tampa, Florida 33620, USA*

(Received 19 February 2016; revised manuscript received 13 July 2016; published 5 August 2016)

Tensile strain along the c_R axis in epitaxial VO₂ films raises the temperature of the metal insulator transition and is expected to stabilize the intermediate monoclinic M2 phase. We employ surface-sensitive x-ray spectroscopy to distinguish from the TiO₂ substrate and identify the phases of VO₂ as a function of temperature in epitaxial VO₂/TiO₂ thin films with well-defined biaxial strain. Although qualitatively similar to our Landau-Ginzburg theory predicted phase diagrams, the M2 phase is stabilized by nearly an order of magnitude more strain than expected for the measured temperature window. Our results reveal that the elongation of the c_R axis is insufficient for describing the transition pathway of VO₂ epitaxial films and that a strain induced increase of electron correlation effects must be considered.

DOI: [10.1103/PhysRevB.94.085105](https://doi.org/10.1103/PhysRevB.94.085105)

The abrupt metal insulator transition (MIT) near room temperature in VO₂ is believed to be a cooperative Mott-Peierls transition, which is further complicated by the appearance of an intermediate insulating phase under certain conditions. This monoclinic M2 phase is a known Mott insulator suggesting that electron-electron interactions may play an important role in determining the transition pathway [1–3]. In unstrained stoichiometric VO₂, the structural phase transition accompanying the MIT is from the high temperature rutile phase to the monoclinic M1 phase, which causes both zigzagging of the vanadium chains and the formation of V-V dimers along the rutile c (c_R) axis [4,5]. In the M2 phase, only half the vanadium chains zigzag, while the other half form V-V dimers [6,7]. This structure is known to be stabilized in large single crystals at intermediate temperatures by low level chemical doping (e.g., with Cr or Al) or uniaxial pressure along the [110] direction, however the electron correlation effects have not been simultaneously investigated [1,2,6,8–10].

Recently, uniaxial strain studies of VO₂ nanobeams have determined that VO₂ has a triple phase point at 65 °C at ambient pressure, where the two insulating monoclinic phases

and the metallic rutile phase can coexist [11,12]. Applying compressive strain along the c_R axis lowers the transition temperature (T_{MIT}), whereas tensile strain along c_R raises the transition to the metallic phase with the M2 phase stabilized between the M1 and rutile phases. In thin films, the M2 phase has only been observed when using symmetry mismatched substrates, which tend to have low lattice strain and high defect concentrations [13–20]. Because of this, no clear relationship between thin film strain and the stabilization of the M2 phase can be deduced from existing reports. Understanding how this phase can be stabilized with epitaxial strain is necessary for a real understanding of how the MIT of VO₂ can be modulated.

Rutile TiO₂ substrates, isomorphic to the metallic phase of VO₂, offer a means to obtain well-defined biaxial tensile strain with lattice mismatches up to a few percent. It is well known that T_{MIT} can be tailored by ± 40 °C by choice of substrate orientation in thin (≤ 40 nm) VO₂/TiO₂ films [21]. This correlates well with tensile or compressive strain along the c_R axis, however there has been no evidence of the M2 phase reported in these films.

Here we present a combined study of polarization and temperature dependent soft x-ray absorption spectroscopy (XAS) with hard x-ray photoelectron spectroscopy (HAXPES) of high quality epitaxial VO₂ films on TiO₂(001) and (100) oriented substrates. Using the sensitivity of XAS at the O

*lpiper@binghamton.edu

†Present Address: Advanced Photon Source, Argonne National Laboratory, Argonne, Illinois 60439, USA.

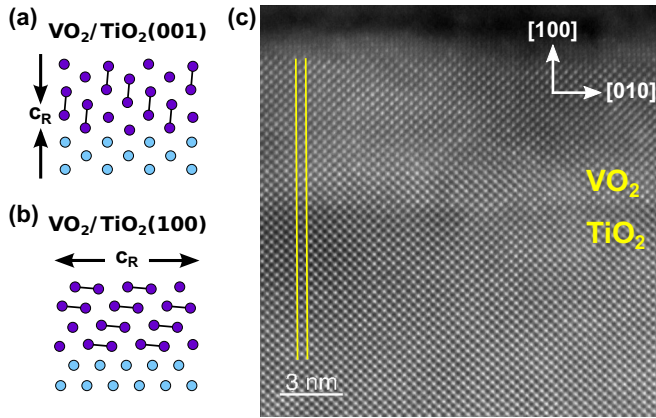


FIG. 1. Schematic representations of the crystal structure of epitaxial VO_2 film grown on (a) $\text{TiO}_2(001)$ and (b) $\text{TiO}_2(100)$, showing the orientation of the V-V dimers. (c) ADF STEM image of a 7.5 nm $\text{VO}_2/\text{TiO}_2(100)$ epitaxial film viewed along the $[001]$ axis.

K edge to the presence of the V-V dimers, we are able to distinguish between each of the three phases (M1, M2, and R). We determine the $\text{VO}_2/\text{TiO}_2(001)$ with a compressed c_R are absent of intermediate phases and maintain a MIT similar to unstrained VO_2 , aside from the lowered T_{MIT} . In stark contrast, the $\text{VO}_2/\text{TiO}_2(100)$ films with elongated c_R have a stable M2 phase between the M1 and R endpoints, while the HAXPES displays evidence of a more Mott-like transition with increased electron correlation effects. These results are generally in good agreement with nonthin film studies, however we note a significantly larger strain than predicted is required to stabilize the M2 phase for the same temperature window. This discrepancy is attributed to additional consequences of the biaxial nature of thin film epitaxial strain and reveals that tailoring the MIT of VO_2 is not exclusively determined by the c_R lattice constant.

A set of high quality epitaxial VO_2 thin films were grown on rutile (001) and (100) TiO_2 single crystal substrates by reactive MBE by a codeposition method under a distilled ozone background pressure [22,23]. The XAS and HAXPES presented here were collected from a representative 10 nm $\text{VO}_2/\text{TiO}_2(001)$ film and a 5 nm $\text{VO}_2/\text{TiO}_2(100)$ film. These thicknesses were chosen to ensure the c_R lattice constant is either contracted or elongated, respectively, as shown schematically in Fig. 1. Details regarding sample growth and characterization as well as spectroscopy measurements are provided in the Supplemental Material [24]. Electrical transport measurements of these films show a change in resistivity of $\Delta R/R = 10^{3.09}$ centered at 19.1°C for $\text{VO}_2/\text{TiO}_2(001)$ and $\Delta R/R = 10^{2.94}$ centered at 77.6°C for $\text{VO}_2/\text{TiO}_2(100)$. This confirms a similar orientation-dependent tuning of the MIT as previously reported [21]. XAS of the O K edge was measured in total electron yield (TEY) mode. The photon energy axes were calibrated using the Ti $L_{2,3}$ and O K absorption edge features of a rutile TiO_2 single crystal. From prior studies we have determined that for films of ≥ 5 nm thickness there is no spectral contamination originating from the TiO_2 substrate [25]. The HAXPES measurements were performed using a photon energy of $h\nu = 4$ keV with a resolution of

0.45 eV. The binding energy axes were referenced to the Fermi edge of Au foil.

For an in-depth analysis of the epitaxial nature of our $\text{VO}_2/\text{TiO}_2(100)$ films, STEM and high resolution XRD measurements were conducted. Cross-sectional scanning transmission electron microscopy (STEM) of $\text{VO}_2/\text{TiO}_2(001)$ specimens have previously shown abrupt interfaces and well-defined epitaxial growth where $(001) \text{VO}_2 \parallel (001) \text{TiO}_2$ and $[100] \text{VO}_2 \parallel [100] \text{TiO}_2$ [22,26]. Here we confirm $\text{VO}_2/\text{TiO}_2(100)$ to have a similarly well-defined epitaxial relation of $(100) \text{VO}_2 \parallel (100) \text{TiO}_2$ and $[001] \text{VO}_2 \parallel [001] \text{TiO}_2$. Figure 1(c) shows an annular dark field STEM image of a $\text{VO}_2/\text{TiO}_2(100)$ specimen viewed along the $[001]$ axis, with a (100) film surface. The film has a top surface layer which looks like it belongs to another phase. This is likely due to ion milling damage induced during sample preparation. The undamaged thickness of the film is 6.9–7.0 nm, and the total thickness of the film is 7.5 nm. In addition to the sharp and well-ordered interface, the whole of the film shows comprehensive structure. As highlighted by the yellow lines, the image shows the columns of vanadium ions maintain their alignment with the titanium ions of the substrate all the way to the damaged surface layer with no sign of dislocations. Additionally, these films display a high quality interface with limited titanium diffusion and maintain MITs in films as thin as 1 nm [22,23,25].

Reciprocal space maps were measured around the $(2,0,0)$ specular and $(2,1,1)$ off-specular Bragg peaks of the $\text{TiO}_2(100)$ substrate and are shown in the Supplemental Material [24]. The VO_2 Bragg peak is overlapped with $\text{TiO}_2(2,1,1)$ peak in the in-plane direction, confirming that the in-plane structure of the VO_2 film is fully strained to the in-plane structure of the substrate. From analysis of the Kiessig fringes along the $(H,0,0)$ direction, using a pseudorutile unit cell, the lattice constant along the surface normal is estimated to be $a_R = 4.47 \text{ \AA}$. This is in good agreement with the intensity profile along the $(H,1,1)$ direction. This indicates that the out-of-plane lattice spacing is indeed contracted from its bulk state in these strained films, demonstrating coherent epitaxial strain. From this we confirm an in-plane tensile strain of $\epsilon_{c_R} = 3.74\%$ and $\epsilon_{b_R} = 0.86\%$ up to a film thickness of 7.5 nm in our $\text{VO}_2/\text{TiO}_2(100)$ films.

In order to monitor the behavior of the V-V dimers across the phase transformations of VO_2 we employed soft XAS. XAS at the O K edge probes the conduction band via dipole transitions into the unoccupied O $2p$ density of states near E_F . Because of the high degree of O $2p$ -V $3d$ covalent mixing, this technique is sensitive to the unoccupied V $3d$ states associated with the formation of V-V dimers [27,28]. This so-called d_{\parallel} feature in the XAS spectrum emerges for the low temperature insulating phase and is routinely considered a signature of the monoclinic M1 structure. Furthermore, since only every other vanadium ion chain forms V-V dimers in the M2 structure, as compared to the full dimerization in the M1 structure, this technique is expected to also be a sensitive probe of the M1/M2 phase transition.

First, polarization dependent XAS was performed for both VO_2 film orientations in the low temperature M1 phase (see the Supplemental Material [24]). The general features in the XAS spectra are consistent with previous studies and show

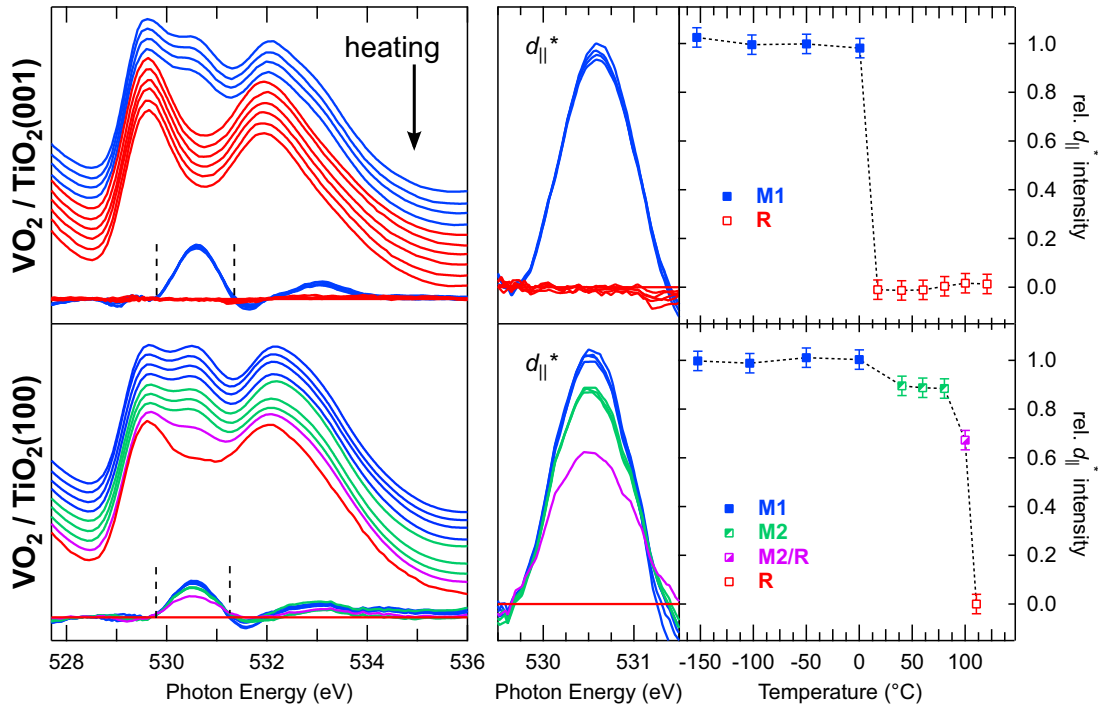


FIG. 2. (Left) Temperature dependent O K -edge XAS measurements of $\text{VO}_2/\text{TiO}_2(001)$ and $\text{VO}_2/\text{TiO}_2(100)$ with (right) an expanded view of the d_{\parallel} feature and its peak intensity as a function of temperature.

no observed energetic shifts or broadening of the unoccupied bands owing to epitaxial strain [27–29]. Due to the highly directional $d_{x^2-y^2}$ orbital, the d_{\parallel} feature shows a strong angular dependence and even completely disappears for polarization geometry $\vec{E} \perp c_R$. Because of this, the d_{\parallel} is slightly less pronounced in the (001) oriented films owing to the constraints of the near grazing incidence geometry required for $\vec{E} \parallel c_R$.

Temperature dependent XAS measurements were then carried out for both VO_2 films and are shown in Fig. 2. Each collected raw spectrum has been normalized to the local maximum of the π^* feature (~ 529.5 eV), and are vertically offset for clarity with temperature increasing from top to bottom. Below these are each difference spectra to represent the spectral changes as temperature is increased. This shows the d_{\parallel} band as a symmetric peak centered at 530.5 eV in both strain orientations.

To highlight the more subtle changes in the d_{\parallel} region, an expanded view is also shown for each film orientation alongside the integrated peak intensity as a function of temperature. The error bars plotted for the integrated peak intensity represent a 99.6% confidence level. From this it is clear that the (001) oriented films display only two phases. The d_{\parallel} feature is identical at all lower temperatures and then vanishes near room temperature and for all higher temperatures. This is consistent with a transition from the M1 to R phase near room temperature with no evidence of any intermediate phases. In contrast, the (100) oriented films display more intricate changes as the temperature is increased. At low temperatures the d_{\parallel} feature is again observed as a symmetric peak, however, in this case, it shows intermediate intensities before it completely vanishes. The first reduction in intensity occurs before 40 °C and remains as a stable plateau at least up to 80 °C. Subsequently, there

is an additional point at which the intensity is diminished further before completely vanishing upon reaching the high temperature phase. The endpoints are similar to the (001) orientation and are consistent with the M1 and R phases. The stable intermediate phase is interpreted as the M2 phase, where the reduced intensity of the d_{\parallel} feature reflects the decreased participation in the V-V dimerization. Following this assignment, the single spectrum collected at 100 °C is likely representative of spatial coexistence between the M2 and rutile phases [24]. This demonstrates that the intermediate M2 phase can indeed be stabilized via coherent epitaxial strain and is only observed in the (100) strain case, i.e., when the c_R lattice constant is elongated.

To confirm the assignment of the intermediate M2 phase observed for the $\text{VO}_2/\text{TiO}_2(100)$ we performed hybrid DFT using the HSE06 functional [30] of the M1, M2, and R phases of VO_2 as described by Eyert [31]. Spin polarization was explicitly included only for the M2 phase in order to obtain a band gap, while the M1 and R calculations are not spin polarized [31,32]. The $t_{2g}(\pi)$ projected density of states for both the M1 and M2 phase are presented in Fig. 3 (see the Supplemental Material for details [24]). The $d_{x^2-y^2}$ orbital, associated with the d_{\parallel} feature in the O K edge, is found at 1.6 eV above E_F in the M1 structure. For the M2 structure, this $d_{x^2-y^2}$ orbital is projected separately for each unique vanadium atom; V1 representing the dimerized chains, and V2 representing the evenly spaced zigzagged chains. The behavior of the unoccupied $d_{x^2-y^2}$ orbital is clearly altered compared to the M1 phase. The lower DOS of this orbital in the M2 phase indeed reflects the reduced participation in the V-V dimerization, reaffirming that the d_{\parallel} feature is largely derived from the dimerized vanadium ions.

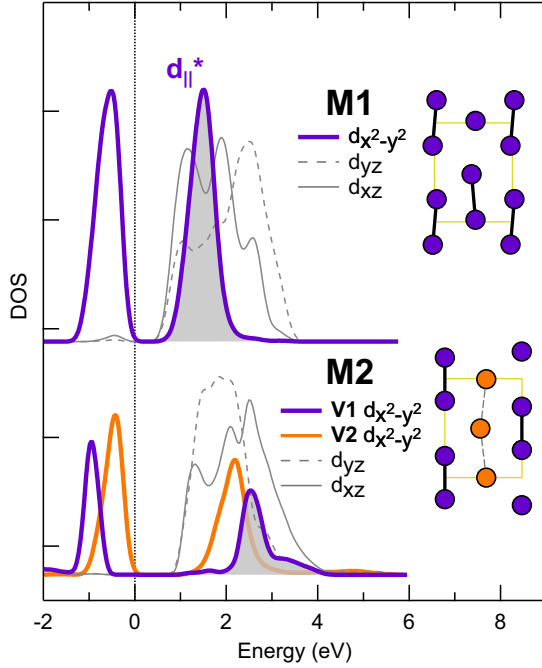


FIG. 3. The $t_{2g}(\pi)$ projected DOS comparing the M1 and M2 phase calculated by hybrid DFT. The highlighted region indicates the $d_{||}$ band in each structure arising from dimerized vanadium ions.

Further confirmation of the existence of the M2 phase in the (100) strained films is supported by Landau-Ginzburg theory. The predicted structural phase transformations in VO_2 as a function of biaxial strain are described here using a six-order Landau polynomial (see the Supplemental Material for details [24])

$$F(\eta, \epsilon) = A2(T - T_C)\eta^2 + A4\eta^4 + A6\eta^6 + \frac{1}{2}c_{ijkl}(\epsilon_{ij} - \eta^2\epsilon_{ij}^0)(\epsilon_{kl} - \eta^2\epsilon_{kl}^0), \quad (1)$$

where T_C is the Curie temperature under stress-free condition, $A2$, $A4$, and $A6$ are constants, η is a normalized order parameter describing the R to M1 transformation, R to M2 transformation, and M2 to M1 transformation, ϵ_{ij} is the total strain, ϵ_{ij}^0 is the stress-free transformation strain at transition temperature T_0 , and c_{ijkl} is the elastic stiffness tensor [33]. For a thin film clamped on the substrate in the x_1 - x_2 plane, by applying the thin film boundary condition we obtain the new transition temperature

$$T_0 = \frac{(A4 + \Delta A4)^2}{4A2A6} + (T_C + \Delta T_C), \quad (2)$$

with $\Delta T_C = \frac{T_0}{\Delta H} [\frac{c_{13}^2}{c_{33}} (\epsilon_{11}^0 + \epsilon_{22}^0) (\epsilon_{S1} + \epsilon_{S2}) - (c_{11}\epsilon_{11}^0 + c_{12}\epsilon_{22}^0)\epsilon_{S1} + (c_{12}\epsilon_{11}^0 + c_{11}\epsilon_{22}^0)\epsilon_{S2}]$ and $\Delta A4 = -\frac{c_{13}^2}{2c_{33}} (\epsilon_{11}^0 + \epsilon_{22}^0)^2 + 2c_{66}\epsilon_{12}^0{}^2 + c_{12}\epsilon_{11}^0\epsilon_{22}^0 + \frac{c_{11}}{2} (\epsilon_{11}^0{}^2 + \epsilon_{22}^0{}^2)$, where ϵ_{S1} and ϵ_{S2} are substrate mismatch strain along x_1 and x_2 directions, respectively. By rotating the coordinate system, we thus can easily get the strain-temperature phase diagrams for both strain cases reflecting epitaxial VO_2 on $\text{TiO}_2(001)$ and (100).

Comparing the tensile sides of each phase diagram in Fig. 4, we find good qualitative agreement with experiment. As the

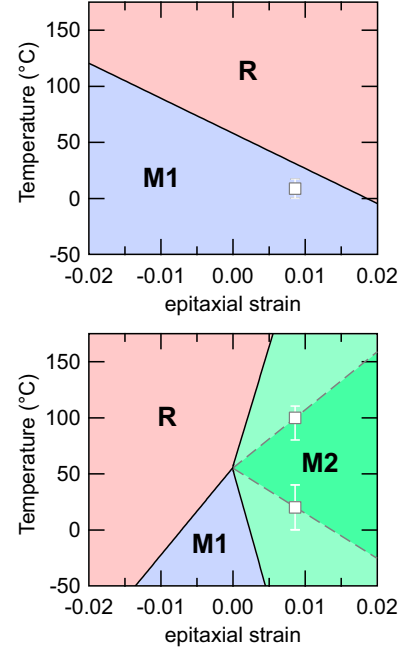


FIG. 4. Transformation temperature as a function of mismatch strain for (001) VO_2 (top) and (100) VO_2 (bottom) thin films. In the (001) case, the epitaxial strain is equal in the a_R and b_R directions, while in the (100) case, the x axis represents the epitaxial strain along the b_R direction (ϵ_{S1}), with the strain along c_R direction (ϵ_{S2}) fixed to $4.35\epsilon_{S1}$ in order to reflect the anisotropic epitaxial strain. The white boxes (along with dotted lines to guide the eye) represent experimentally determined transformation temperature values.

temperature increases, M1 transforms to R directly in (001) films, while M1 transforms first to M2 and then to R in (100) films. The M2 phase has a larger stress-free transformation strain (1.57%) along c_R than that of M1 (1.00%), thus the large c_R tensile strain of the (100) films should favor the M2 phase over M1 and stabilize it for a wide temperature range. However, the epitaxial strain of a (100) film is very anisotropic, i.e., 0.86% along the b_R direction and 3.74% along c_R , and we find significant differences in experimental transformation temperatures. For this measured temperature window in which the M2 phase is stable, the strain on c_R observed in our films is nearly an order of magnitude higher than expected. This large discrepancy indicates that the effects of biaxial epitaxial strain alone are insufficient to accurately describe these phase transformations. There may be additional consequences to the epitaxial strain, such as changes in bandwidth and thus correlation strength that may have a large impact on the transformation temperatures.

To investigate any such modification to the electronic structure in the highly anisotropic $\text{VO}_2/\text{TiO}_2(100)$ strain case, we employed HAXPES. Figure 5 shows the HAXPES spectra of the topmost valence band states for each film orientation recorded both above and below their respective T_{MIT} (as determined from resistivity measurements). The valence band of VO_2 consists of a broad O $2p$ band (2–9 eV) and a smaller feature near E_F that is predominantly V $3d$ in character (see the Supplemental Material for full VB spectra [24]). This V $3d$ feature displays dramatic changes across the MIT. Here we

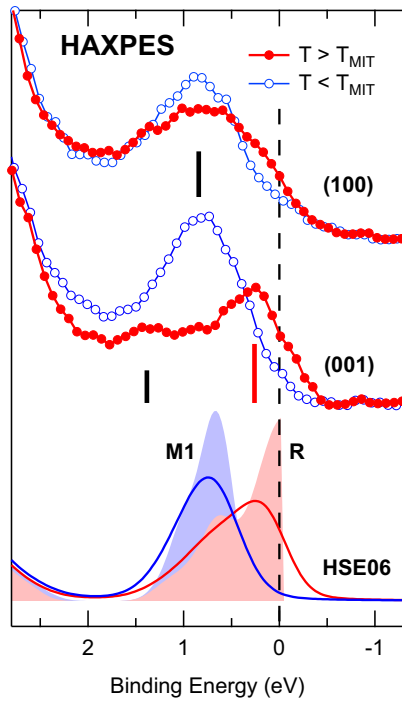


FIG. 5. Valence band HAXPES of $\text{VO}_2/\text{TiO}_2(100)$ and $\text{VO}_2/\text{TiO}_2(001)$ collected above and below T_{MIT} . (Bottom) HSE06 hybrid DFT calculations showing the total DOS for the M1 and R phase. Solid bars indicate the coherent (red) and incoherent (black) contributions to the V $3d$ feature.

also observe clear differences between the two strain cases. The $\text{VO}_2/\text{TiO}_2(001)$ spectra shows a single peak near 1 eV in the insulating phase that shifts towards E_F above T_{MIT} resulting in a clear metallic Fermi edge. This is consistent with our hybrid DFT predicted spectra, and shows the (001) oriented films are in good agreement with bulk VO_2 and other reports of $\text{VO}_2/\text{TiO}_2(001)$ [28,29,34–36]. Also in the metallic phase, there is some additional weight above 1 eV that is not captured in the DFT band calculations. This broad feature is the so-called “incoherent peak” associated with the lower Hubbard band [35].

Now looking to the $\text{VO}_2/\text{TiO}_2(100)$ spectra for the metallic phase, this incoherent peak is much more pronounced and is observed at the same binding energy as the insulating peak, near 1 eV. In this case, there is only a small transfer of spectral weight across the MIT resulting in small density of states at E_F in the metallic phase and is consistent with previous observations of $\text{VO}_2/\text{TiO}_2(100)$ films [25,37]. This behavior is more typical of a Mott insulating system, indicating that the electron correlations are more dominant in the (100) oriented films [38,39]. Doping VO_2 with tungsten has also been observed to induce more Mott-like spectral signatures, although in the present case these effects are purely strain induced [40]. This increase in electron correlation effect is likely a consequence of the distortion of the rutile phase induced by the epitaxial strain in $\text{VO}_2/\text{TiO}_2(100)$ films. We consider this to be responsible for the discrepancy between the predicted and observed phase transformation temperatures. Further support is provided by a strain-induced orbital selective

Mott transition explicitly considering the effects of electron correlations in VO_2 , as proposed by Mukherjee *et al.* [41].

We have demonstrated here that the intermediate M2 phase can indeed be stabilized via coherent epitaxial strain where the c_R axis is elongated. This result can largely be explained by the change in c_R lattice constant, however the temperature window in which the M2 phase is stable is quantitatively different than predicted for $\text{VO}_2/\text{TiO}_2(100)$ films. This discrepancy is a consequence of the increased electron correlations in the $\text{VO}_2/\text{TiO}_2(100)$ films as compared to $\text{VO}_2/\text{TiO}_2(001)$, indicating that the more Mott-like MIT character needs to be explicitly considered. Due to the well-defined epitaxial strain in these films, we can now provide an explanation for the inconsistent appearance of the M2 phase in thin VO_2 films where the biaxial strain and possible renormalization of the electronic structure are not explicitly considered. This work demonstrates that by use of epitaxial strain, it may be possible to further strain-tune the degree of electron correlation in VO_2 .

We thank J. A. Moyer and P. Schiffer for assistance with the transport measurements. We thank W.-C. Lee and S. Mukherjee for fruitful discussions. L.F.J.P. and N.F.Q. acknowledge support from the National Science Foundation under DMR 1409912. The work of H.P. and D.G.S. was supported in part by the Center for Low Energy Systems Technology (LEAST), one of the six SRC STARnet Centers, sponsored by MARCO and DARPA. The HAXPES and XAS measurements presented in the main text were performed at beamlines X24A and U4B, respectively, at the National Synchrotron Light Source. Additional HAXPES and XAS measurements were performed at beamlines 6.3.1.2 ISAAC of the Advanced Light Source (ALS) and I09 at Diamond Light source. The NSLS is supported by the U.S. Department of Energy, Office of Science, Office of Basic Energy Sciences, under Contract No. DE-AC02-98CH10886. The work at ALS is supported by the Office of Basic Energy Sciences, of the U.S. Department of Energy under Contract No. DE-AC02-05CH11231. We thank Diamond Light Source for access to beamline I09 (SI12546) that contributed to the results presented here. Cornell High Energy Synchrotron Source (CHESS) is supported by the National Science Foundation and the National Institutes of Health/National Institute of General Medical Sciences under NSF award DMR-1332208. M.E.H. is funded by Department of Energy BES DE-SC0002334. This work made use of the electron microscopy facility of the Cornell Center for Materials Research with support from the National Science Foundation (NSF) Materials Research Science and Engineering Centers program (DMR 1120296) and NSF IMR-0417392. This work made use of the ARCHER UK National Supercomputing Service (<http://www.archer.ac.uk>), via the membership of the UKs HPC Materials Chemistry Consortium, which is funded by EPSRC (EP/L000202). A.M.G. acknowledges Diamond Light Source for the co-sponsorship of a studentship on the EPSRC Centre for Doctoral Training in Molecular Modeling and Materials Science (EP/L015862/1). B.J.M. acknowledges support from the Royal Society (UF130329). Y.G., F.X., and L.Q.C. acknowledge support from the Penn State MRSEC, Center for Nanoscale Science, under the award NSF DMR-1420620.

- [1] J. P. Pouget, H. Launois, T. M. Rice, P. Dernier, A. Gossard, G. Villeneuve, and P. Hagenmuller, *Phys. Rev. B* **10**, 1801 (1974).
- [2] J. P. Pouget, H. Launois, J. P. D'Haenens, P. Merenda, and T. M. Rice, *Phys. Rev. Lett.* **35**, 873 (1975).
- [3] T. M. Rice, H. Launois, and J. P. Pouget, *Phys. Rev. Lett.* **73**, 3042 (1994).
- [4] F. J. Morin, *Phys. Rev. Lett.* **3**, 34 (1959).
- [5] J. B. Goodenough, *J. Solid State Chem.* **3**, 490 (1971).
- [6] M. Marezio, D. B. McWhan, J. P. Remeika, and P. D. Dernier, *Phys. Rev. B* **5**, 2541 (1972).
- [7] V. Eyert, *Ann. Phys.* **11**, 650 (2002).
- [8] J. B. Goodenough and H. Y. P. Hong, *Phys. Rev. B* **8**, 1323 (1973).
- [9] G. Villeneuve, M. Drillon, J. C. Launay, E. Marquestaut, and P. Hagenmuller, *Solid State Commun.* **17**, 657 (1975).
- [10] J. P. Pouget and H. Launois, *J. Phys.* **37**, 49 (1976).
- [11] J. Cao, Y. Gu, W. Fan, L. Q. Chen, D. F. Ogletree, K. Chen, N. Tamura, M. Kunz, C. Barrett, J. Seidel *et al.*, *Nano Lett.* **10**, 2667 (2010).
- [12] J. H. Park, J. M. Coy, T. S. Kasirga, C. Huang, Z. Fei, S. Hunter, and D. H. Cobden, *Nature (London)* **500**, 431 (2013).
- [13] D. G. Schlom, L.-Q. Chen, C.-B. Eom, K. M. Rabe, S. K. Streiffer, and J.-M. Triscone, *Annu. Rev. Mater. Res.* **37**, 589 (2007).
- [14] K. Okimura, T. Watanabe, and J. Sakai, *J. Appl. Phys.* **111**, 073514 (2012).
- [15] D. Fu, K. Liu, T. Tao, K. Lo, C. Cheng, B. Liu, R. Zhang, H. A. Bechtel, and J. Wu, *J. Appl. Phys.* **113**, 043707 (2013).
- [16] S.-H. Kim, B.-J. Kim, T.-Y. Jeong, Y.-S. Lee, and K.-J. Yee, *J. Appl. Phys.* **117**, 163107 (2015).
- [17] K. Okimura, N. Hanis Azhan, T. Hajiri, S. I. Kimura, M. Zaghrioui, and J. Sakai, *J. Appl. Phys.* **115**, 153501 (2014).
- [18] Y. Ji, Y. Zhang, M. Gao, Z. Yuan, Y. Xia, C. Jin, B. Tao, C. Chen, Q. Jia, and Y. Lin, *Sci. Rep.* **4**, 4854 (2014).
- [19] H. W. Yang, J. I. Sohn, J. H. Yang, J. E. Jang, S. N. Cha, J. Kim, and D. J. Kang, *Europhys. Lett.* **109**, 27004 (2015).
- [20] N. H. Azhan, K. Su, K. Okimura, M. Zaghrioui, and J. Sakai, *J. Appl. Phys.* **117**, 245314 (2015).
- [21] Y. Muraoka and Z. Hiroi, *Appl. Phys. Lett.* **80**, 583 (2002).
- [22] H. Paik, J. A. Moyer, T. Spila, J. W. Tashman, J. A. Mundy, E. Freeman, N. Shukla, J. M. Lapano, R. Engel-Herbert, W. Zander *et al.*, *Appl. Phys. Lett.* **107**, 163101 (2015).
- [23] H. Paik, J. Moyer, J. Tashman, M. Jerry, N. Shukla, W. Zander, J. Schubert, R. Engel-Herbert, S. Datta, P. Schiffer *et al.* (unpublished).
- [24] See Supplemental Material at <http://link.aps.org/supplemental/10.1103/PhysRevB.94.085105> for additional details regarding sample growth and characterization, supporting HAXPES and XAS spectra, details of the Landau-Ginzburg and DFT calculations, and includes Refs. [42–47].
- [25] N. F. Quackenbush, H. Paik, J. C. Woicik, D. A. Arena, D. G. Schlom, and L. F. J. Piper, *Materials (Basel)* **8**, 5452 (2015).
- [26] J. W. Tashman, J. H. Lee, H. Paik, J. A. Moyer, R. Misra, J. A. Mundy, T. Spila, T. A. Merz, J. Schubert, D. A. Muller *et al.*, *Appl. Phys. Lett.* **104**, 063104 (2013).
- [27] M. Abbate, F. M. F. de Groot, J. C. Fuggle, Y. J. Ma, C. T. Chen, F. Sette, A. Fujimori, Y. Ueda, and K. Kosuge, *Phys. Rev. B* **43**, 7263 (1991).
- [28] T. C. Koethe, Z. Hu, M. W. Haverkort, C. Schüßler-Langeheine, F. Venturini, N. B. Brookes, O. Tjernberg, W. Reichelt, H. H. Hsieh, H. J. Lin *et al.*, *Phys. Rev. Lett.* **97**, 116402 (2006).
- [29] N. F. Quackenbush, J. W. Tashman, J. A. Mundy, S. Sallis, H. Paik, R. Misra, J. A. Moyer, J. H. Guo, D. A. Fischer, J. C. Woicik *et al.*, *Nano Lett.* **13**, 4857 (2013).
- [30] A. V. Krukau, O. A. Vydrov, A. F. Izmaylov, and G. E. Scuseria, *J. Chem. Phys.* **125**, 224106 (2006).
- [31] V. Eyert, *Phys. Rev. Lett.* **107**, 016401 (2011).
- [32] R. Grau-Crespo, H. Wang, and U. Schwingenschlögl, *Phys. Rev. B* **86**, 081101 (2012).
- [33] Y. Gu, J. Cao, J. Wu, and L.-Q. Chen, *J. Appl. Phys.* **108**, 083517 (2010).
- [34] S. Shin, S. Suga, M. Taniguchi, M. Fujisawa, H. Kanzaki, A. Fujimori, H. Daimon, Y. Ueda, K. Kosuge, and S. Kachi, *Phys. Rev. B* **41**, 4993 (1990).
- [35] A. Fujimori, I. Hase, Y. Tokura, M. Abbate, J. C. Fuggle, H. Eisaki, and S. Uchida, *Phys. B* **186-188**, 981 (1993).
- [36] R. Eguchi, M. Taguchi, M. Matsunami, K. Horiba, K. Yamamoto, Y. Ishida, A. Chainani, Y. Takata, M. Yabashi, D. Miwa *et al.*, *Phys. Rev. B* **78**, 075115 (2008).
- [37] J. Laverock, A. R. H. Preston, D. Newby, K. E. Smith, S. Sallis, L. F. J. Piper, S. Kittiwatanakul, J. W. Lu, S. A. Wolf, M. Leandersson *et al.*, *Phys. Rev. B* **86**, 195124 (2012).
- [38] A. Fujimori, I. Hase, H. Namatame, Y. Fujishima, Y. Tokura, H. Eisaki, S. Uchida, K. Takegahara, and F. M. F. de Groot, *Phys. Rev. Lett.* **69**, 1796 (1992).
- [39] M. Imada, A. Fujimori, and Y. Tokura, *Rev. Mod. Phys.* **70**, 1039 (1998).
- [40] E. Sakai, K. Yoshimatsu, K. Shibuya, H. Kumigashira, E. Ikenaga, M. Kawasaki, Y. Tokura, and M. Oshima, *Phys. Rev. B* **84**, 195132 (2011).
- [41] S. Mukherjee, N. F. Quackenbush, H. Paik, C. Schlueter, T.-L. Lee, D. G. Schlom, L. F. J. Piper, and W.-C. Lee, *Phys. Rev. B* **93**, 241110 (2016).
- [42] Y. Yamamoto, K. Nakajima, T. Ohsawa, Y. Matsumoto, and H. Koinuma, *Jpn. J. Appl. Phys.* **44**, L511 (2005).
- [43] C. Dallera, L. Braicovich, L. Duò, A. Palenzona, G. Panaccione, G. Paolicelli, B. C. C. Cowie, and J. Zegenhagen, *Nucl. Instrum. Methods Phys. Res. Sect. A* **547**, 113 (2005).
- [44] G. Kresse and J. Hafner, *Phys. Rev. B* **47**, 558(R) (1993).
- [45] G. Kresse and J. Hafner, *Phys. Rev. B* **49**, 14251 (1994).
- [46] G. Kresse and J. Furthmüller, *Phys. Rev. B* **54**, 11169 (1996).
- [47] G. Kresse and J. Furthmüller, *Comput. Mater. Sci.* **6**, 15 (1996).